General Disclaimer

One or more of the Following Statements may affect this Document

- This document has been reproduced from the best copy furnished by the organizational source. It is being released in the interest of making available as much information as possible.

- This document may contain data, which exceeds the sheet parameters. It was furnished in this condition by the organizational source and is the best copy available.

- This document may contain tone-on-tone or color graphs, charts and/or pictures, which have been reproduced in black and white.

- This document is paginated as submitted by the original source.

- Portions of this document are not fully legible due to the historical nature of some of the material. However, it is the best reproduction available from the original submission.

NATIONAL AERONAUTICS AND SPACE ADMINISTRATION

Technical Memorandum 33-755

Simulation of an Ion Thruster Control System

I. Kudo

Electrotechnical Laboratory

Tokyo, Japan

L. C. Pless and E. V. Pawlik

Jet Propulsion Laboratory

JET PROPULSION LABORATORY

CALIFORNIA INSTITUTE OF TECHNOLOGY

PASADENA, CALIFORNIA

February 15, 1976

NATIONAL AERONAUTICS AND SPACE ADMINISTRATION

Technical Memorandum 33-755

Simulation of an Ion Thruster Control System

I. Kudo

Electrotechnical Laboratory

Tokyo, Japan

L. C. Pless and E. V. Pawlik

Jet Propulsion Laboratory

JET PROPULSION LABORATORY

CALIFORNIA INSTITUTE OF TECHNOLOGY

PASADENA, CALIFORNIA

February 15, 1976

PREFACE

The work described in this report was performed by the Propulsion Division of the Jet Propulsion Laboratory.

CONTENTS

I. Introduction 1

II. Thruster Operation 2

III. Control Model 5

A. Ion Beam Current -- Main Vaporizer Loop 6

B. Discharge Voltage -- Cathode Vaporizer Loop 7

C. Neutralizer Keeper Voltage -- Neutralizer Vaporizer Loop 8

IV. Control Loop Analysis 9

A. Steady-State Operation 9

B. Throttling 11

C. Runaway Conditions 13

V. Conclusions 14

References 15

APPENDIX

A. Computer-Program Listing for the Ion Thruster Model 35

TABLES

1. Normal thruster operating parameters 16

2. Ion thruster description 17

FIGURES

1. 700 series thruster 18

2. Discharge chamber schematic 18

3. Power processor grounding 19

4. Block diagram of thruster control loop 20

5a. Block diagram - main vaporizer loop 21

FIGURES

5b. Block diagram - cathode vaporizer loop 21
5c. Block diagram - neutralizer vaporizer loop 21
6. Beam characteristics 22
7. Main vaporizer heater supply characteristics 22
8. Vaporizer time constant (bell jar tests) 23
9. Mass flow rate vs temperature 23
10. Vaporizer heater characteristics 24
11. Discharge characteristics 24
12. Discharge chamber characteristics 25
13. Measured flow rate characteristics 25
14. Cathode loop heater characteristics 26
15. Neutralizer keeper characteristics 26
16. Typical computer runs showing the effect of the environmental temperature 27
17. Loop oscillations vs temperature at typical beam current (1.0 A) 28
18. Loop oscillations vs temperature at typical beam current (1.5 A) 28
19. Loop oscillations vs temperature at typical beam current (2.0 A) 28
20. Comparison of discharge voltage ripple 29
21. Oscillations using a constant slope supply 29
22. Loop oscillations using a constant power supply 30
23. Discharge supply characteristics plotted on thruster characteristics 30
24. Comparison of simulated and actual step responses 31
25. Discharge characteristics showing the effect of I_D/I_B ratio 32
26. Runaway recovery characteristics when using a constant current discharge supply 32
27. Flow rate vs beam current for a constant discharge current supply 33
28. Runaway recovery characteristics with zero delay times 33
29. Flow rate vs beam current 34
30. Runaway recovery characteristics when using a 6 V/A discharge supply 34

ABSTRACT

This report describes the results of an initial effort at Jet Propulsion Laboratory (JPL) to model the control loops of a 30-cm diameter electron bombardment thruster and a transistorized power processor so as to predict its operation. Data, from which the model is made, are presented as well as comparisons between the computer outputs and test data from the JPL Solar Electric Propulsion systems laboratory.

I. INTRODUCTION

Ion thrusters are at the state of development where they are being considered for use for primary spacecraft propulsion (Refs. 1-3) and for earth-orbital applications (Refs. 4 and 5). The effort at JPL has been directed toward the use of 30-cm diameter ion thrusters for primary propulsion on a solar electric spacecraft. A computer simulation of the thruster control system, therefore, became of increasing interest in order to: (1) examine thruster operation as a function of expected variations in control loop parameters and thruster environment, (2) construct a model of the thrust subsystem for use in mission operations, and (3) examine interactions between the thruster and the solar array.

The control of ion thrusters can, in general, be separated into two categories. The first deals primarily with the control of the thrust level after steady-state operating temperatures are reached. The second deals with bringing the thruster on line and monitoring its operation. The first category is covered in this report. The second, which uses a digital computer for timing and event monitoring, is discussed in Refs. 6 and 7.

The work described in this paper represents the initial stages of the effort to simulate the thruster control loops. The model was constructed using characteristic data, as available, from the latest 30-cm ion thrusters supplied from Hughes Research Laboratories for testing at JPL. Data was obtained initially from a modified 400 series thruster (Ref. 8). Some of the thruster characterizations were later updated to include data from a 700 series engineering model thruster (Ref. 9). These data were used along with the control functions incorporated in a transistorized power processor of the type described in Ref. 10 to construct a model of the operation of the thruster control system. These loops were analyzed to determine the extent of the effect of control-loop parameters and the thruster thermal environment on control stability and accuracy. The model analysis places the most emphasis on the very low frequency effects introduced by the thruster. It does not include the high frequency oscillations normally present in the thruster discharge, since these oscillations are beyond the control-loop response frequencies.

II. THRUSTER OPERATION

Figures 1 and 2 are cutaway views of the thruster modeled. Liquid mercury propellant is vaporized in separate feed systems for the propellant distributor, ion source chamber cathode, and neutralizer. At present, thrusters operate with about 88% of the flow supplied to the propellant distribution manifold, 10% to the discharge cathode, and 2% to the discharge neutralizer. Electrons are drawn out of the high-density mercury plasma formed in the discharge cathode by the keeper electrode. These electrons are then dispersed by the baffle plate and accelerated into the main discharge chamber by a positive anode voltage. When in the main discharge chamber, these energetic electrons ionize the neutral propellant mercury and form a mercury plasma. The divergent magnetic field, created by the magnets and soft-iron pole pieces, traps the ionizing electrons and enhances the ionization process. Ions formed in the discharge chamber drift toward the screen electrode. When passing through the plasma sheath, the ions are accelerated through the concentric holes in the screen and accelerator electrodes by the applied electric field. The ion beam is then decelerated by the space charge forces in the ion beam to a potential slightly higher than the ambient-space plasma potential and neutralized by the electrons emitted by the discharge neutralizer. Over a relatively wide range of thruster performance, thrust is directly proportional to the mass flow rate of vaporized propellant into the thruster. The thrust, T, is a function of ion beam current and screen voltage as shown by the equation:

$$T = KI_B \sqrt{V_s - V_p}$$

where

I_B = ion beam current

K = constant

V_s = screen voltage

V_p = plasma voltage

To throttle the ion engine, the flow rate of propellant into the thruster can be varied or the screen voltage can be varied. Propellant throttling is the normal mode used in order to simplify the power processor design.

The neutralizer is quite similar to the cathode used to supply electrons to the main discharge chamber; however, it requires a much lower flow of mercury vapor to operate.

The thruster is surrounded by a cover at the spacecraft-frame potential to prevent the space plasma or neutralizing electrons from being drawn to the high-positive potential of the thruster body and creating severe power losses.

There are three control loops required to operate the thruster. The main vaporizer is used as the primary control on the thrust level. Beam current is sensed and used to control the power to heat the main vaporizer. The discharge power is also controlled. Control of the propellant-utilization factor (the ratio of the mass of the ions expelled to the propellant input mass) is accomplished by setting the discharge current level and the discharge voltage is controlled to a fixed level to limit the ion erosion rate at the cathode. Thirdly, the neutralized ion beam couples to the ambient-space plasma through a potential drop of several volts. This potential drop is indirectly controlled by regulating the keeper voltage by adjusting the neutralizer flow rate.

A magnetic baffle is used to affect the impedance between the cathode and anode, thereby influencing the discharge stability. This magnetic baffle around the cathode is clearly shown in Figs. 1 and 2. The magnetic field from this coil is used to restrict the flow of electrons from the cathode to the anode and thereby alter the main discharge chamber direct current characteristics (this effect is not built into the present model because of the limited amount of data available at this time).

One other point of interest can be seen in Figs. 1 and 2. The main vaporizer drives an isolator followed by a propellant distributor, while the cathode vaporizer drives an isolator and tubing to the centrally located cathode. All of these volumes introduce transport lags into the loops and tend to introduce low-frequency oscillations.

Figure 3 is a block diagram of the proposed Power Processor (PP) required to operate the thruster and the interconnections within the thruster. The primary purposes of the PP are: (1) to interface between a high-impedance source and the thruster, (2) to provide all power supplies required by the thruster, and (3) to protect both itself and the thruster from electrical failure. There are twelve supplies required to operate and start the thruster (not all on at the same time). The screen supply is the major supply (2 A at 1100 V) with the discharge supply next (12 A at 37 V). All of the rest (except for the accelerator supply) are low-voltage, low-power supplies. The accelerator normally runs at 500 V, 0.004 A. Normal operating conditions for the thruster are listed in Table 1.

III. CONTROL MODEL

A simulation of the control loops for a 30-cm diameter ion thruster is being developed at Jet Propulsion Laboratory in the form of a computer model. The simulation uses Continuous System Simulation Language (CSSL)[1], and closes the loop by iteration between sets of measured data. The thruster and power processor supply characteristics are included within the model.

Figure 4 shows a block diagram of the control components in a thruster-power processor set. This diagram is broken up and presented in a greater detail in Fig. 5. Most empirical thruster data used in the model were derived using a modified Hughes S/N 404 thruster. Some of the 400 series data has been updated by using information obtained with a Hughes S/N 703 thruster. A description of these thrusters is contained in Table 2. The characteristics of a transistorized power processor of Ref. 10 are used. This unit was modified for operation with the 30-cm thruster.

The model contains three major loops. These loops are: (1) the ion beam current-main vaporizer loop which controls primarily the thrust level, (2) the discharge voltage-cathode vaporizer loop which controls the discharge chamber voltage, and (3) the neutralizer keeper voltage-neutralizer vaporizer loop which controls both the amount of mercury flow through the neutralizer and the potential of the exhaust plume. The first two loops (the beam current and the discharge voltage) interact through the mass flow that each provides to the discharge chamber and by the power supplied to the discharge. All vaporizers are affected by the thermal environment and this effect is included in the model. The effect of variations in the magnetic baffle current, screen voltage, and acceleration voltage is not included at this time. The computer-program listing for the model is included in Appendix A. Additional details of each of the three loops are described in the following sections.

---

[1] Programming Sciences Corporation, Los Angeles, CA.

A. ION BEAM CURRENT -- MAIN VAPORIZER LOOP

This loop is shown in Fig. 5a. The beam current is determined by the total mass flow rate and the power supplied to the discharge. This loop controls the main vaporizer flow rate and is affected by the cathode vaporizer flow rate from the discharge loop. The empirical relationship for the thruster characteristics as used in this loop is shown in Fig. 6, where the total mass flow rate is expressed as the sum of the main and the cathode flow rates ($\dot{m}_M + \dot{m}_C$). A reference level for the thrust level is supplied to this loop in the form of an ion beam reference (I_B ref.). The error signal is acted on by the vaporizer heater controller to heat the main vaporizer. This controller, whose characteristics are shown in Fig. 7, is normally a proportional device that saturates at large error levels. This controller determines the value of the main vaporizer heater current. The applied heater power controls the vaporizer temperature. The vaporizer has a thermal transfer function $G_2(S)$ which can be represented by a first-order lag with a time constant of 250 s.

The resulting vaporizer temperature rise, when added to the temperature of the vaporizer environment (TE 2), determines the vaporizer operating temperature. Experimental results for determining the vaporizer time constant are presented in Fig. 8. The heating and cooling time constants are very close as can be seen by the slopes of the normalized heating and cooling curves. Typical vaporizer curves are shown in Fig. 9. The relationship between the vaporizer heater power and the rise in vaporizer temperature is presented in Fig. 10.

Vaporized mercury leaving the porous tungsten surface flows into the discharge chamber through a high-voltage isolator, and then through a manifold which introduces some delay time. This main vaporizer flow rate affects the discharge loop by changing the effective cathode mass flow rate, $\dot{M}_c$, as follows: $\dot{M}_c = \dot{m}_c + K\dot{m}_M$ where K is an experimentally determined weighting factor.

The ion beam current, as can be seen in Fig. 6, is not a monotonic function of total mass flow rate. The control loops will not function properly when the slope of the curve is negative. Another thruster parameter, accelerator current, is used to indicate when this condition exists, since

it is primarily a function of propellant utilization. An override is, therefore, included in the loop to turn the main vaporizer power off at an accelerator current of 10 mA and to restore loop operation when the accelerator current drops below 6 mA. The override levels were chosen to correspond to the experimental work presented in Ref. 11.

B. DISCHARGE VOLTAGE -- CATHODE VAPORIZER LOOP

This loop is shown in Fig. 5b. In this loop the discharge voltage is maintained at a level where minimum cathode erosion will occur. The electrical impedance of the discharge chamber is a function of both the discharge current and the effective mass flow rate ($\dot{M}_c$). Empirical relationships for these chamber characteristics are presented in Figs. 11 and 12. The experimentally determined value of K that was used for the beam-loop interaction was 0.133 and was determined by using flow rate data. More recent data on the 703 thruster indicate that K is closer to 0.126 and may be a function of beam and discharge currents. The requirement for this K factor may best be seen in Fig. 13, where, for a constant ratio of discharge current to beam (5), the cathode flow rate decreases as the discharge and beam currents are increased. To keep the discharge voltage constant, one would expect the cathode flow rate to increase as the current is increased. However, the coupling from the main vaporizer causes the discharge control loop to lower the cathode flow rate. The factor K may be determined with the following procedure. With the beam off, the cathode and main flow rates required to keep the discharge voltage constant over the range of discharge current required are measured. The sum of these flow rates is defined as $\dot{M}_c$. Then, with the beam on, the flow rates are measured. Then, for corresponding discharge currents, $K = (\dot{M}_c - \dot{m}_c)/\dot{m}m$, where $\dot{m}_c$ and $\dot{m}m$ are the flow rates measured with the beam on.

A discharge supply provides the propellant-ionizing power to the discharge chamber. As suggested in Ref. 10, the discharge supply V-I characteristics may be varied in order to study the effects of power supply and thruster interactions. Several characteristics were investigated, including constant current, V to I ratios of both (-) 3 and (-) 6 V/A, and constant power. The effects of changing the V-I characteristics will be

examined in this report. The operating level of the controlled voltage sets the discharge power for a corresponding beam-current level, usually at a ratio of 5:1, discharge current to beam current. This loop, therefore, controls the thruster efficiency.

The discharge voltage is sensed at the output of the discharge supply and is compared with a normally fixed reference level. Voltage signals are acted on by a controller which adjusts a power supply to heat the cathode vaporizer. The characteristics of this controller are presented in Fig. 14. Thermal effects are included in the same manner as for the beam loop. The mercury flow again encounters a transport lag due to flow restrictions in the isolator, propellant line, and cathode.

C. NEUTRALIZER KEEPER VOLTAGE -- NEUTRALIZER VAPORIZER LOOP

This loop is shown in Fig. 5c. The mass flow rate through the neutralizer is controlled by maintaining the keeper voltage constant. The flow rate is affected by the current drawn to the keeper electrode. The neutralizer characteristics used in this loop are shown in Fig. 15. The potential of the exhaust plasma is also indirectly controlled by this loop. It is a function of both the mass flow rate and the keeper current. In maintaining the flow rate, the keeper voltage is compared against a normally fixed reference level. Error signals, as in the case of the above loops, are used to adjust the mercury flow rate from the vaporizer. This vaporizer is also affected by the temperature of the environment, TE_3. Very small delay times may exist due to the neutralizer isolator and cathode.

In the laboratory, there is some interaction between the beam-current level and the neutralizer keeper voltage. There is little data available, and since the coupling is thought to be a function of the keeper supply V-I characteristic, this effect is not included in the model.

IV. CONTROL LOOP ANALYSIS

The computer model was used to perform some preliminary analysis of the thruster operation under both steady-state and transient conditions. In addition, the runaway conditions, under which a thruster escapes from the control loops, and the restoring mechanism were examined. Each of these three areas is described below. Experimental results of the thruster control-loop operation were used both to compare and to guide the modifications to the model. Operation of the neutralizer was not included in the results described below.

A. STEADY-STATE OPERATION

Thruster operation has been observed to contain small oscillations (approximately 3 to 5%) in the beam current and discharge voltage. Some attempts at minimizing this type of oscillation have been presented in Ref. 10. The control-loops were, therefore, parametrically examined to determine conditions under which these oscillations may exist. The results indicate that if there is no delay time, there would be no oscillations over the range of loop gains used in the JPL laboratory. Introduction of delay times in both loops will cause small oscillations in the discharge and beam loops. The amplitude of the oscillations was found, within a small temperature range, to be a function of the delay time. This analysis was performed for a low gain (1A/V) in the discharge loop and a high gain (110 A/A) in the beam loop. These settings are representative of current thruster operating conditions.

An investigation of the effects of increasing the discharge-loop gain showed that the amplitude of the discharge oscillations increased rapidly as the discharge-loop gain was increased to greater than 2.0. These oscillations were coupled into the beam current. The investigation of variations in the beam-loop gain was not completed. Lowering the gain below approximately 90 A/A resulted in poor beam-current regulation.

Identical delay times were used in each of the two thruster control loops. The beam-current oscillation waveforms are shown in Fig. 16 as a function of time for main and cathode loop delay times of 1.0 s. The effects

of different levels of temperature environment are also included. (In the figures, temperatures are in millivolts output from a Type E (Chromel - Constantan) thermocouple). The amplitude of these oscillations are plotted against the temperature environment of the main and cathode vaporizer in Figs. 17-19. Nominal operating temperatures of the main and cathode vaporizers are also indicated in the figures. It can be seen that the oscillations are zero for a high-temperature environment (234°C or higher) and increase with decreasing temperature. A region of maximum amplitude was found to exist in each case with the amplitude increasing with larger delay times. The delay times for the 700 series thruster were experimentally found to be about 1 s for the main and discharge loops. These delay times were measured (one at a time) by opening the loops and stepping up the vaporizer currents. The vaporizer temperatures and the controlled parameters were recorded, and the delay time was taken as the time interval between the start of the increase in vaporizer temperature and the start of the change in the controlled parameter.

This procedure is inexact, since there is an unknown time lag between the change in vaporizer temperature and the change in the thermocouple output. More work is required in this area, because the vaporizer flow rate is an exponential function of temperature and the actual temperature does start changing before the thermocouple output does. Thus, the delay time used is too long. This is pessimistic, since in closed-loop systems an increase in the time delay increases the tendency toward instability (a Nyquist diagram is rotated clockwise, or, in the frequency domain, the phase lag is increased proportional to frequency (Ref. 12)).

The characteristics of the discharge power supply were also investigated to determine the effect of this supply on the oscillations. Three discharge supply characteristics are presented. These are: (1) a constant discharge voltage to discharge current ratio of 6 V/A, representing a linear approximation of a constant power discharge supply; (2) a constant current supply, and (3) a constant power output supply. The oscillations in the discharge voltage are compared in Fig. 20 for constant current and linear discharge supplies. A 50% reduction in amplitude was found to exist in the oscillations when using the linear supply. Figures 21 and 22 provide a comparison of the oscillations using linear and constant power output

supplies, respectively. Variations in the cathode loop delay times had little effect on the waveshape.

As expected, the constant power output supply minimizes the oscillations. Figure 23a is a replot of Fig. 11 with the discharge supply characteristics added. For the same variation in mass flow rate, the discharge power change is less for the linear supply than for the constant current supply, and is zero for the constant power supply. Figure 23b is a portion of Fig. 6 showing these discharge variations coupled into the beam current. The flat slope of the constant power curve minimizes the coupling into the beam current.

These results agree with experience in the laboratory. The supply used was "tuned" for minimum ripple, and when its V-I characteristic was measured, it was constant power over the voltage range of interest.

B. THROTTLING

The control-loop operation was examined during the transient condition that occurs in response to a change in thrust level. The response of some parameters in the model and some actual parameters is shown in Fig. 24.

The differences between the simulations and the actual tests are due to (1) the difference in the magnitudes of the steps, and (2) differences between the model and the actual power supply available in the laboratory. The differences in the magnitude of the steps is roughly 2:1. Both the model and the laboratory results are higher than would be used in flight, since such steps would impose severe transients upon a flight power subsystem. The magnitude of the steps in the model was an exploratory attempt at understanding the model, while the laboratory results when trying to duplicate the model were a practical limitation, since the thruster discharge would cease conducting if steps greater than those presented were tried. The work on reconciling the differences is the reason for the author's opinions.

In Figs. 24a and 24c the results of a step increase in beam and discharge currents is shown. The striking differences are in the magnitudes of the transient in the discharge voltage and the time required for the beam current to reach the new value. Addressing the voltage change first,

$$^{2}\frac{\Delta VDM}{\Delta IDM} = \frac{6.7}{2.5} = 2.6, \text{ and } \frac{\Delta VDA}{\Delta IDA} = \frac{1}{1} = 1$$

Assuming a relatively constant DC plasma resistance due to time lags in the mass-flow rates the steps are in reasonable agreement, if the finite response time of the actual supply is considered. The time difference is thought to be caused by a hardware problem. The PP used for the laboratory tests is a modified 20-cm PP (Ref. 10). The major changes that had been made were rebuilding the discharge, screen, and accelerator supplies. The other supplies were left mainly unchanged, since the major effort at JPL concerned interfacing the TSS with a spacecraft, and plans were in process to procure new PPs designed for this thruster. Thus, the vaporizer supplies were power limited at a level lower than used in the model. Since the vaporizer power-temperature and temperature-flow rate characteristics are both exponential functions, the limitations in the power supply could explain the time difference.

The difference in time response in the throttling down example is thought to be due to the difference in magnitude of the change in temperature required. The upward pulse at the beginning of the actual downward step is unexplained. During the testing, it was there most of the time. It may or may not be in the model; the computation interval used was actually longer than the length of this pulse, so the model may have missed this pulse.

There is one other difference between the model and actual hardware. The step functions in the model are instantaneous, while, due to filtering delays, etc., the actual discharge supply took a finite time to step the current. The model should be changed to be more representative.

As the discharge-current to beam-current ratio is reduced (typically to 5:1), runaway occurs more often. The reason for this can be seen in Fig. 25, where, the higher the ratio, the farther the operating region is from the unstable region. The dividing line between the stable region

---

[2] ΔVDM = model change in discharge voltage
ΔVDA = actual change in discharge current, etc.

and the unstable region is the locus of points in Fig. 6 where the slopes of the constant discharge power curves become negative. Note in Fig. 25 that a constant current discharge supply has the shortest path to travel to the unstable region in case of a perturbation in the discharge. It would move vertically, while other V-I characteristics would move parabolically or with a smaller slope.

C. RUNAWAY CONDITIONS

If thruster operation is shifted to the portion of the curves in Fig. 6 where the slope is negative, then the loops will no longer function correctly and the main vaporizer power will be supplied at the maximum level of the supply. This condition has been referred to as "runaway" or "low-mode" operation by various investigators. Several thruster parameters can be used to indicate when this condition occurs. One of the most sensitive appears to be the accelerator current. A controller that operates as a function of the accelerator current was therefore introduced in the loops (Fig. 5a) to restore proper control-loop operation if runaway occurs. This controller turns off the main vaporizer when the accelerator current is greater than 10 MA and restores loop operation when the accelerator current falls below 6 MA. These current amplitudes were suggested in Ref. 12.

In the model, using a constant current discharge supply and a 1-s time delay, if a momentary runaway is forced it will not restabilize as is shown in Figs. 26-29. Figure 26 shows the beam current and discharge voltage variations as a function of time after the initial runaway. This run was terminated by a computer run-time limitation without ever stabilizing. Figure 27 is a variation of a phase plane plot showing beam current and main vaporizer flow rate as a function of time. The returns from the high flow rate conditions were caused by the runaway trip switch. Figures 28 and 29 are similar plots of these parameters obtained under the same conditions except that the delay times were set to zero. After some large oscillations, the run did stabilize with small oscillations in both beam current and discharge voltage.

Figure 30 shows the computer outputs when a discharge supply with a 6 V/A slope and delay times of one second were used. The beam current and discharge voltage stabilize rapidly, followed by oscillations of less than 1%.

V. CONCLUSIONS

A hybrid model of 30-cm ion thruster and transistorized power processor was formulated and programmed on a digital computer. This model was exercised over a range of parameters and the result led to the following conclusions:

(1) The control loops, as presented, are stable for normal values of loop gains when propellant line delay times are zero.

(2) Small oscillations will exist in the loops when representative thruster delay times are included in the model. The amplitudes are on the order of 3% as normally present during thruster operation. They were found to be a function of delay time, loop gains, and the thermal environment near the vaporizer.

(3) Discharge supply characteristics can affect the control-loop oscillations. A constant power discharge supply is most effective in minimizing these oscillations.

(4) The model quantitatively predicts transient operation.

(5) Recovery from runaway can be aggravated by delay time, and to a greater extent, discharge supply characteristics. A constant power discharge supply was found to improve recovery characteristics.

The results of this initial work appear to be a useful tool in understanding control-loop phenomena. Continuation of this type of effort should provide an optimization of the runaway-recovery techniques, and eventually provide a model able to duplicate parameter variations that may occur during a mission using solar electric propulsion.

REFERENCES

1. Duxbury, J. H. and Paul, G. M., Interplanetary Spacecraft Design Using Solar Electric Propulsion, AIAA paper 74-1084, American Institute of Aeronautics and Astronautics, New York, October 1974.

2. Feasibility Study for a Solar Electric Propulsion Stage, Report no. SD 72-5A-0177, North American Rockwell Space Division, Seal Beach, California, January 1973.

3. SERT D Spacecraft Study, NASA TMX-71494, NASA, Lewis Research Center, Cleveland, Ohio, undated.

4. Holcomb, L. B. and De Grey, S. P., Application of Selection Techniques to Electric Propulsion Options on an Advanced Synchronous Satellite, AIAA paper 73-1257, American Institute of Aeronautics and Astronautics, New York, November 1973.

5. Kudo, I., Murakami, H., and Nakayama, K., "Development of Electron Bombardment Ion Engine," J. Japan Society of Aerospace Sciences, Vol. 21, No. 234, p. 393, 1973.

6. Macie, T. W., and Doupe, H. M., Automatic Control of an Electric Thrust Subsystem, AIAA paper no. 72-506, AIAA 9th Electrical Propulsion Conference, Bethesda, Maryland, April 17-19, 1972, American Institute of Aeronautics and Astronautics, New York.

7. Macie, T. W., and MacMedan, M. L., Automatic Control of a Primary Electric Thrust Subsystem, AIAA paper no. 75-381. American Institute of Aeronautics and Astronautics, New York, March 1975.

8. Ion Device Physics Department Staff of Hughes Research Laboratories, Low Voltage 30-cm Ion Thrusts, NASA CR-120919, National Aeronautics and Space Administration, Washington, February, 1972.

9. Poeschel, R. L., King, H. J., and Schnelker, D. E., An Engineering Model 30-cm Ion Thruster, AIAA paper no. 73-1084, AIAA 10th Electric Propulsion Conference, Lake Tahoe, Nevada, October 31 - November 2, 1973, American Institute of Aeronautics and Astronautics, New York.

10. Masek, T. D., Solar Electric Propulsion Thrust Subsystem Development (SEPST III), JPL Technical Report 32-1579, Jet Propulsion Laboratory, Pasadena, California, March 15, 1973.

11. Terdan, F. F., and Bechtel, R. J., Control of a 30-cm Diameter Mercury Bombardment Thruster, AIAA paper no. 73-1079, American Institute of Aeronautics and Astronautics, New York, October 1973.

12. Truxal, J. G., Control System Synthesis, pp. 551-553, McGraw-Hill, New York, 1955.

Table 1. Normal thruster operating and measured parameters

Parameter	Operating point
Discharge voltage reference	37 V
Discharge current reference	5 A
Beam current reference	1 A
Delay time for main vaporizer	1 s
Delay time for cathode vaporizer	1 s
Cathode vaporizer heater gain	1 A/V
Main vaporizer heater gain	110 A/A
Magnetic baffle	40.5 ampere-turns

Table 2. Ion thruster description

Thruster	Baseline	Grids	Electron Baffle	Neutralizer
S/N 404	Ref. 9	Replaced flat grids with curved grids 0.5% compensation 0.15 cm dia accel holes	Increased to 5.87 cm dia	No change
S/N 703	Ref. 10	0.4% compensation in place of 0.5% compensation	Increased to 5.40 cm dia	400 series with electrical isolator

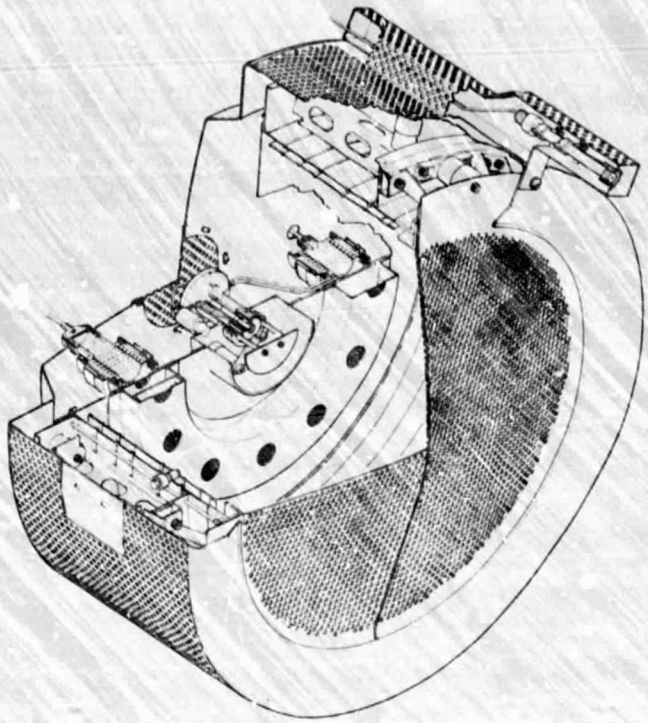

Fig. 1. 700 series thruster

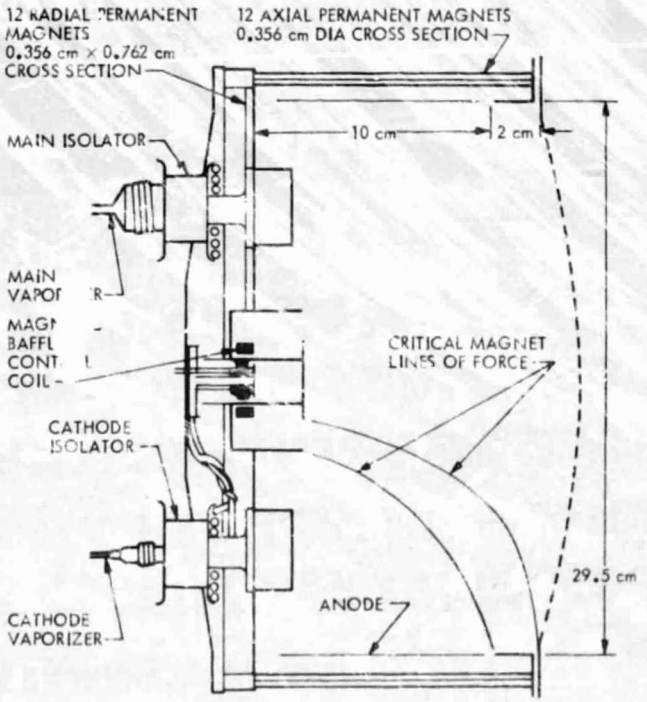

Fig. 2. Discharge chamber schematic

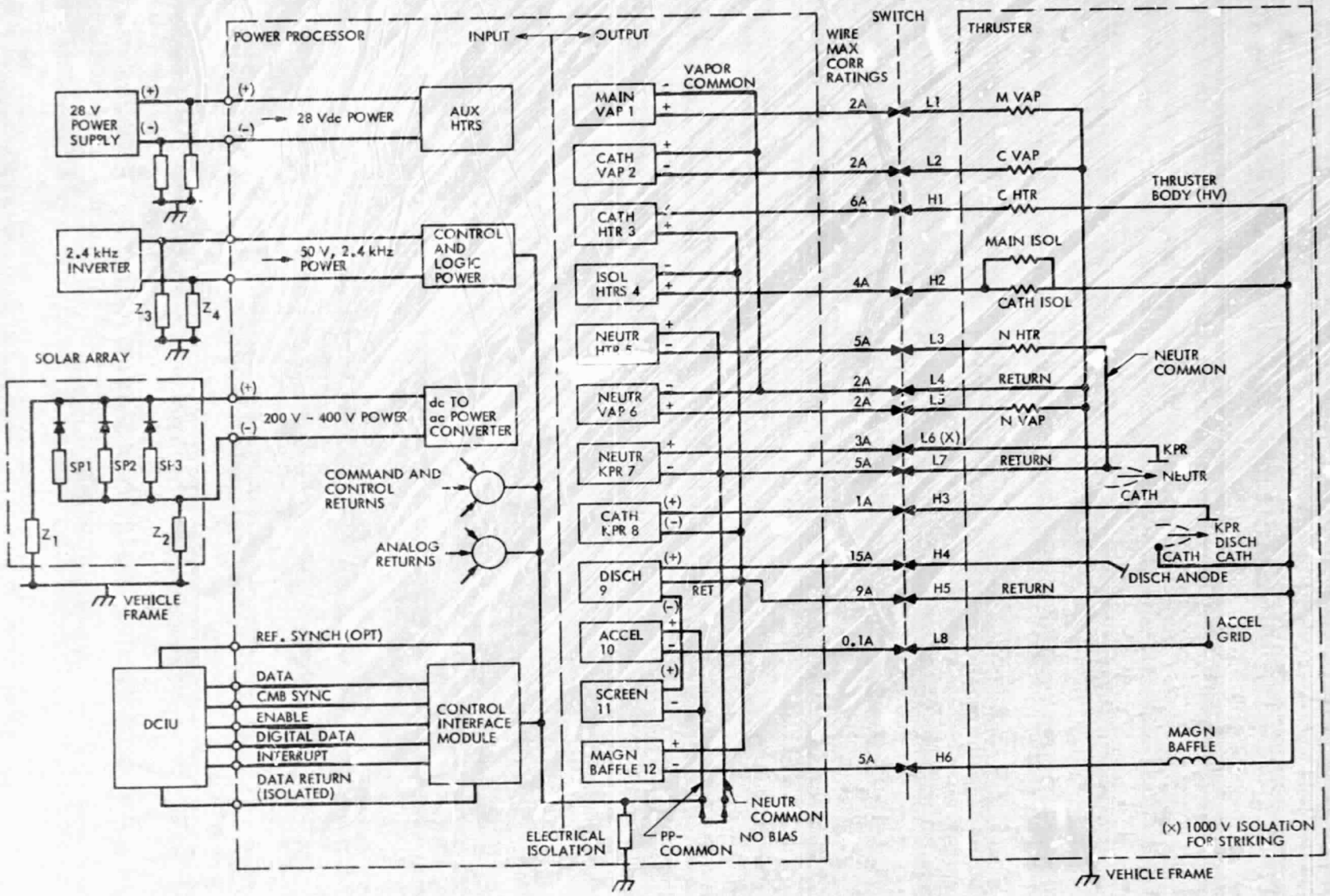

Fig. 3. Power processor grounding

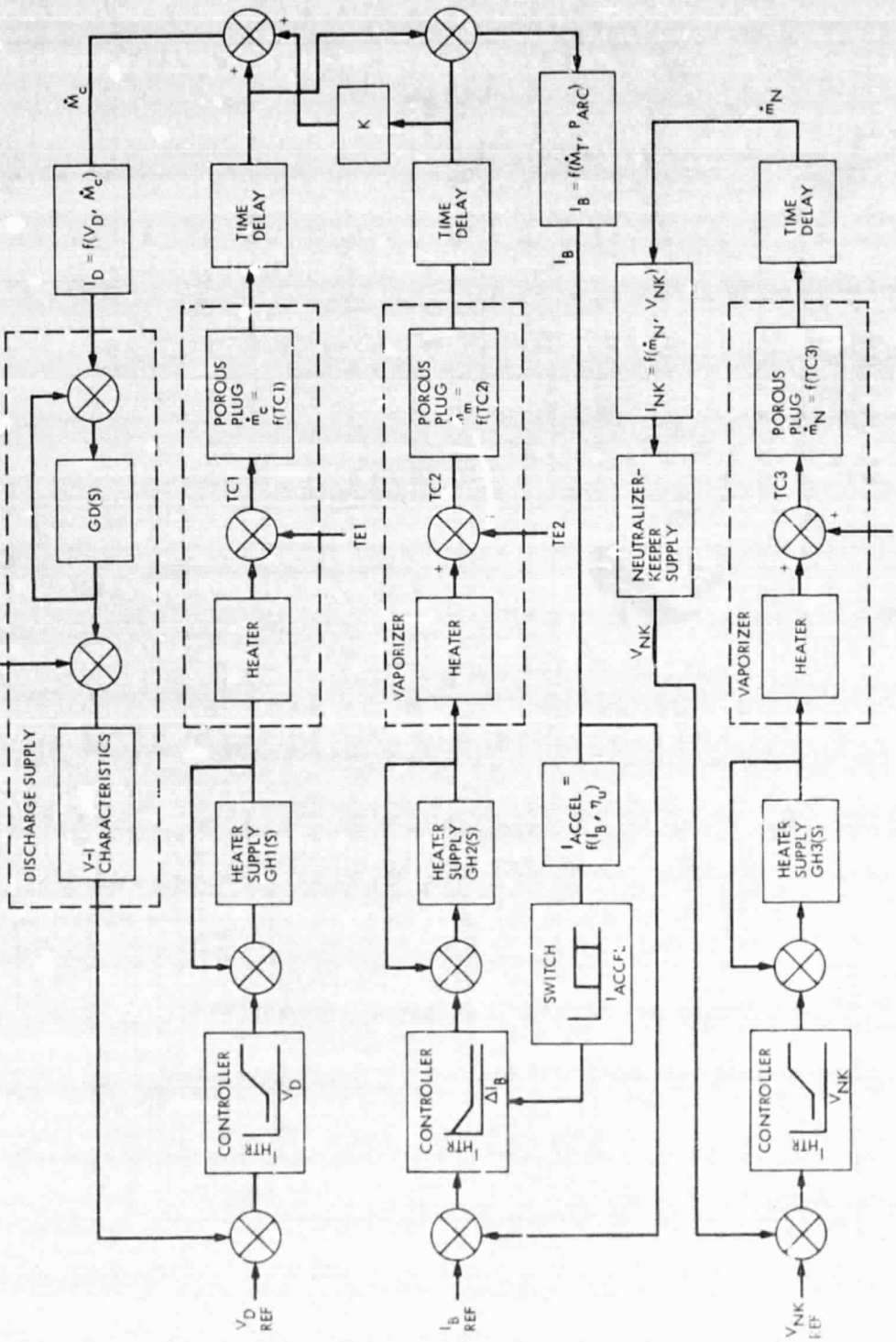

Fig. 4. Block diagram of thruster control loop

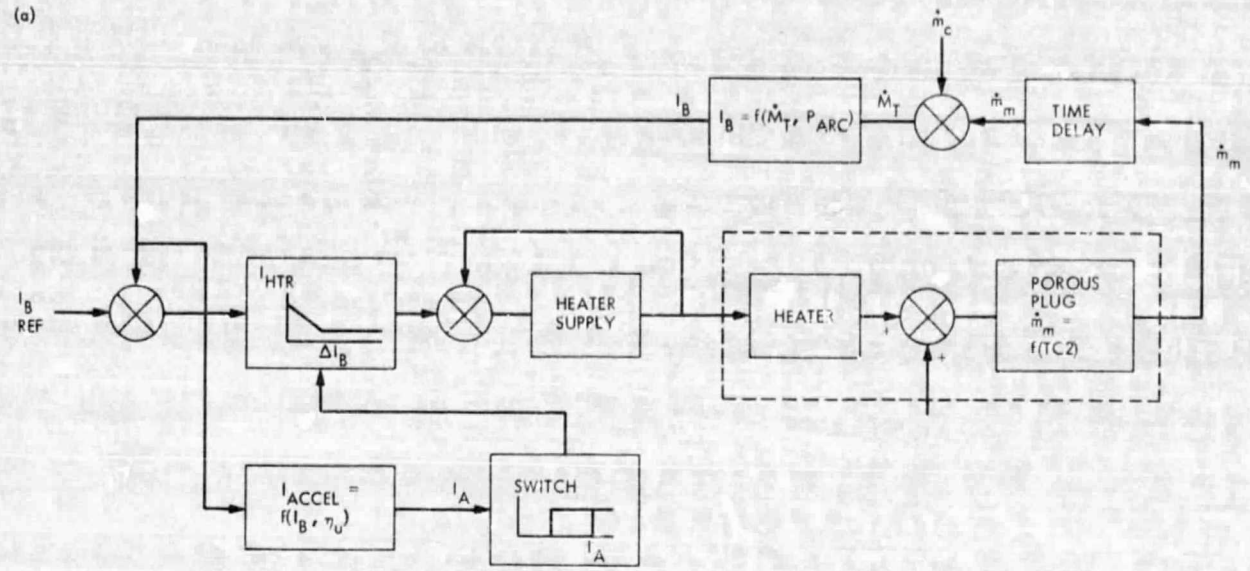

Fig. 5a. Block Diagram - main vaporizer loop

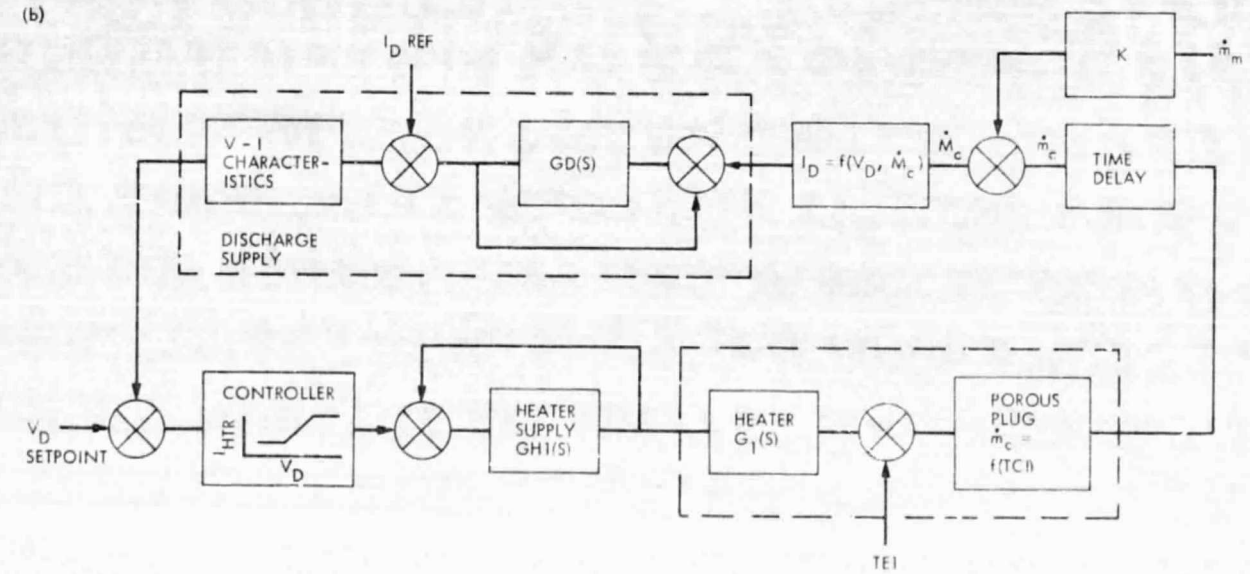

Fig. 5b. Block diagram - cathode vaporizer loop

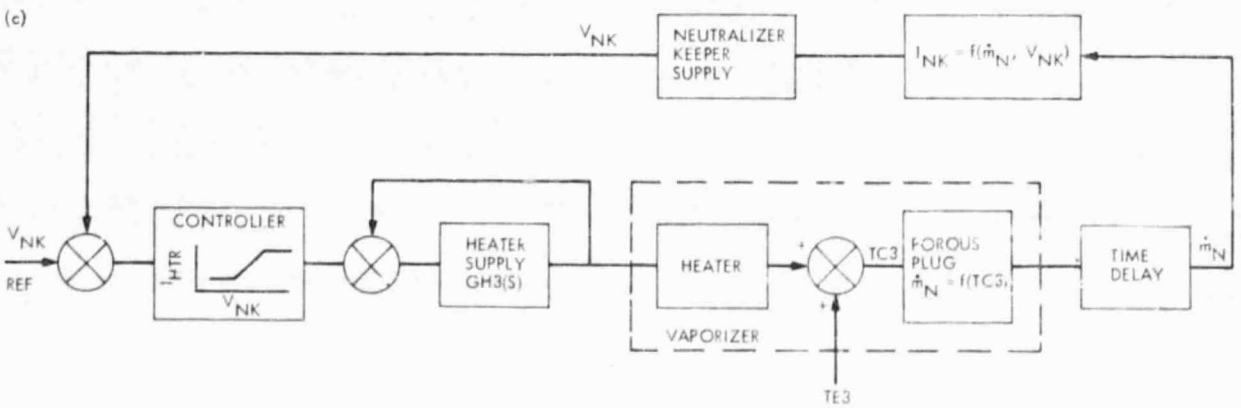

Fig. 5c. Block diagram - neutralizer vaporizer loop

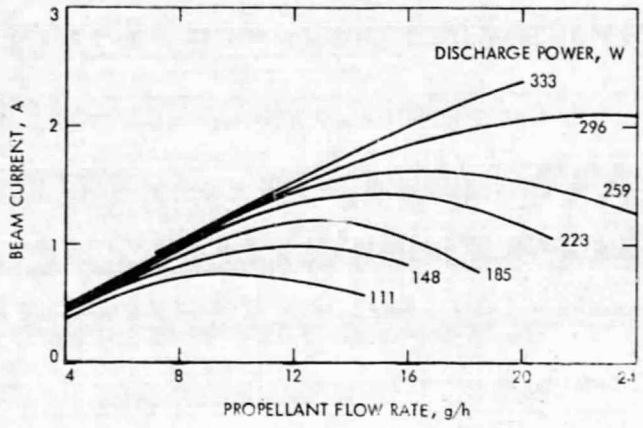

Fig. 6. Beam characteristics

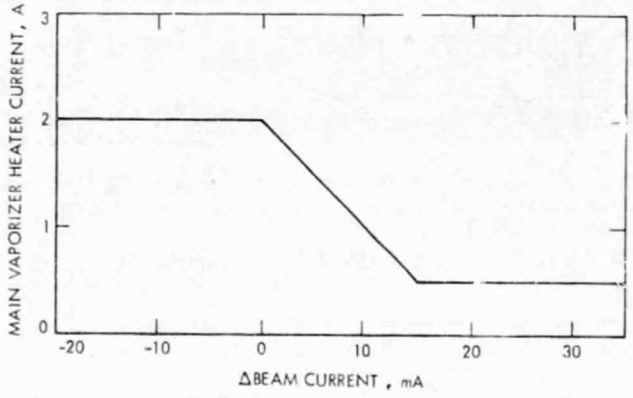

Fig. 7. Main vaporizer heater supply characteristics

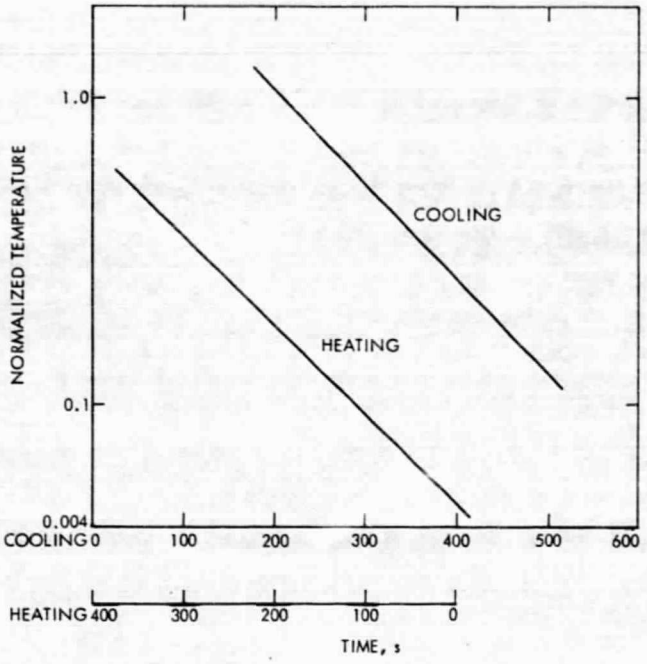

Fig. 8. Vaporizer time constant (bell jar tests)

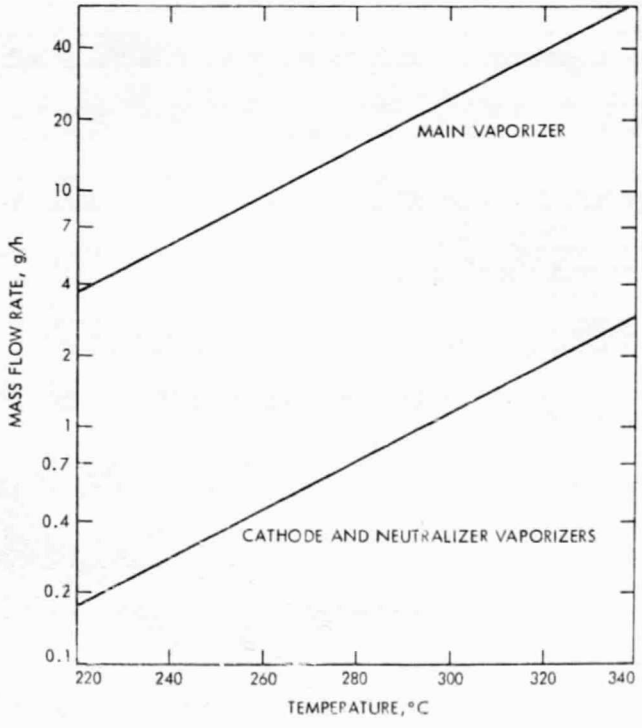

Fig. 9. Mass flow rate vs temperature

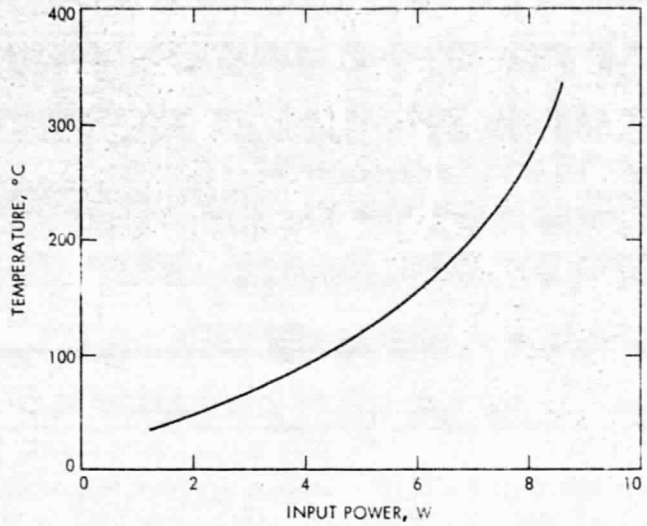

Fig. 10. Vaporizer heater characteristics

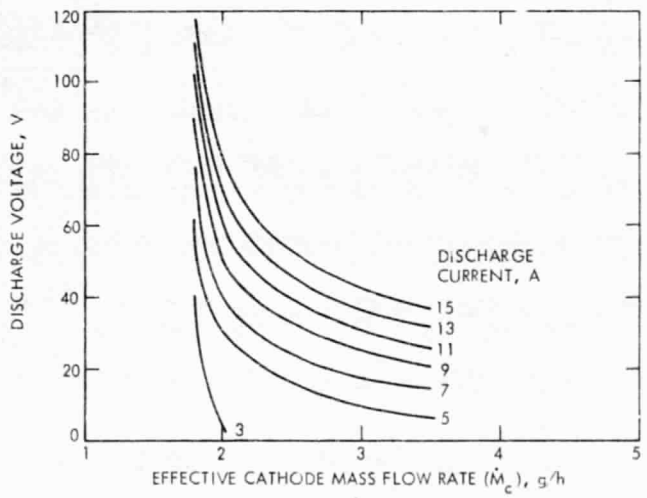

Fig. 11. Discharge characteristics

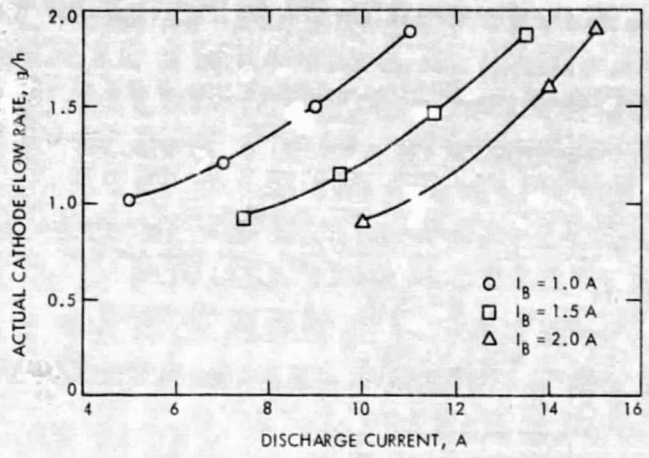

Fig. 12. Discharge chamber characteristics

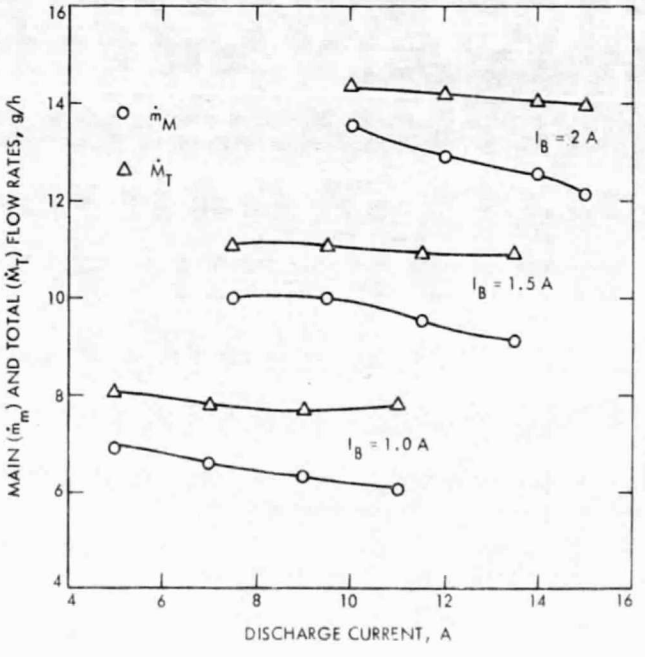

Fig. 13. Measured flow rate characteristics

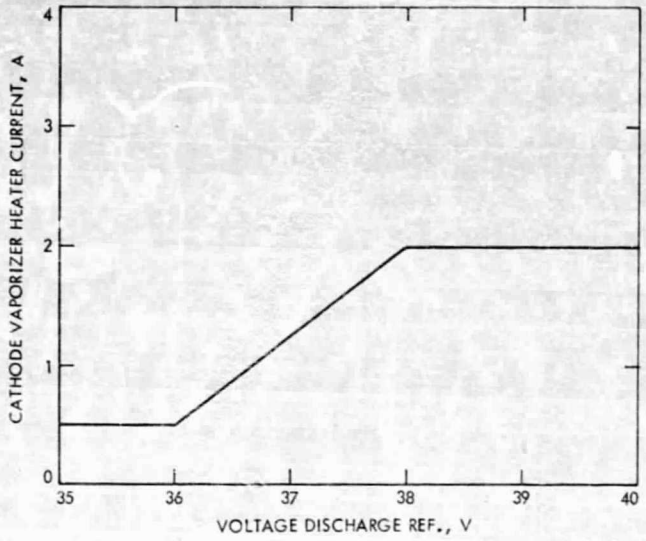

Fig. 14. Cathode loop heater characteristics

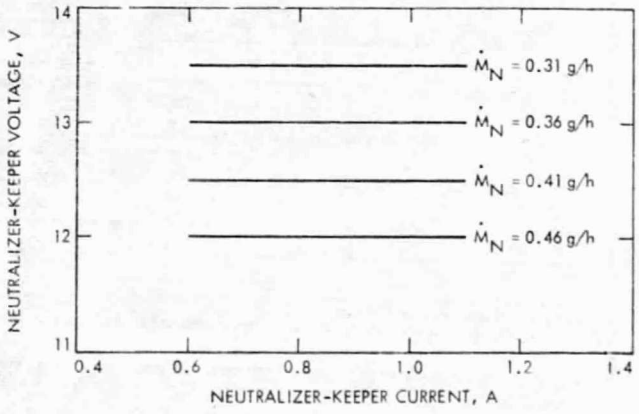

Fig. 15. Neutralizer keeper characteristics

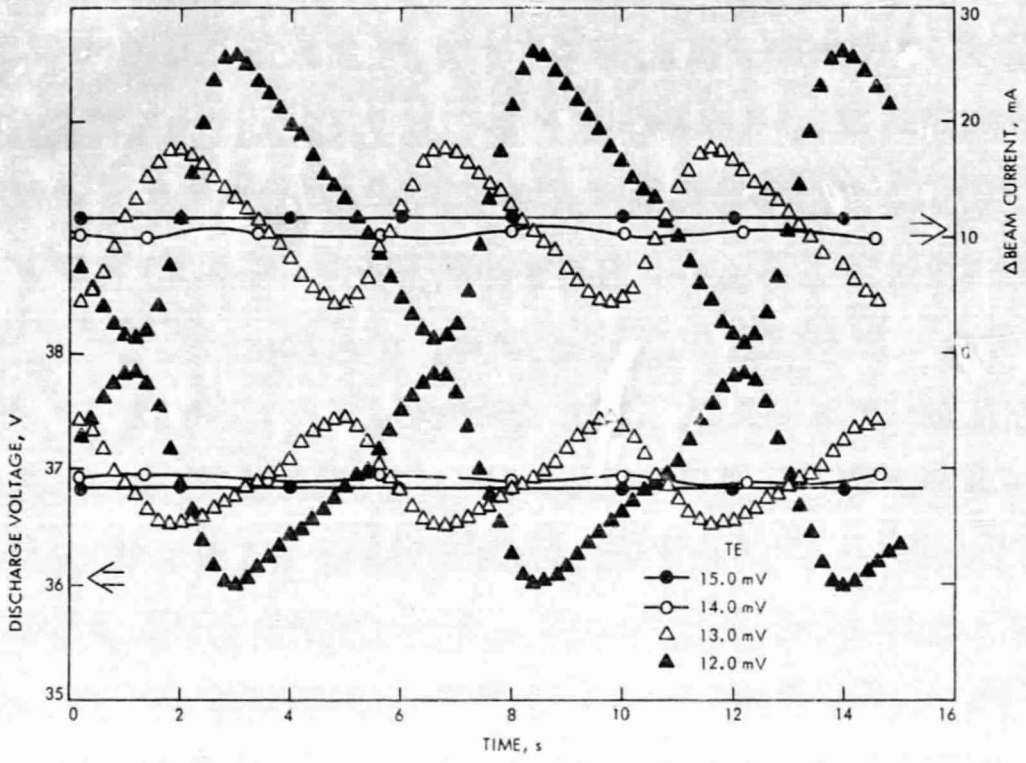

Fig. 16. Typical computer runs showing the effect of the environmental temperature

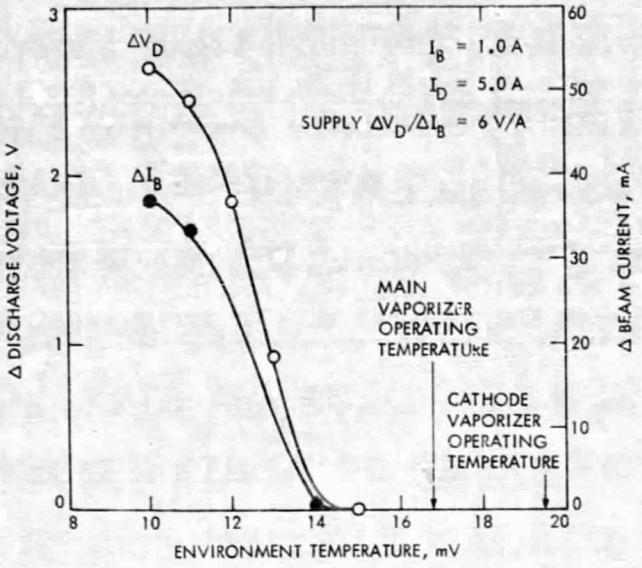

Fig. 17. Loop oscillations vs temperature at typical beam current (1.0 A)

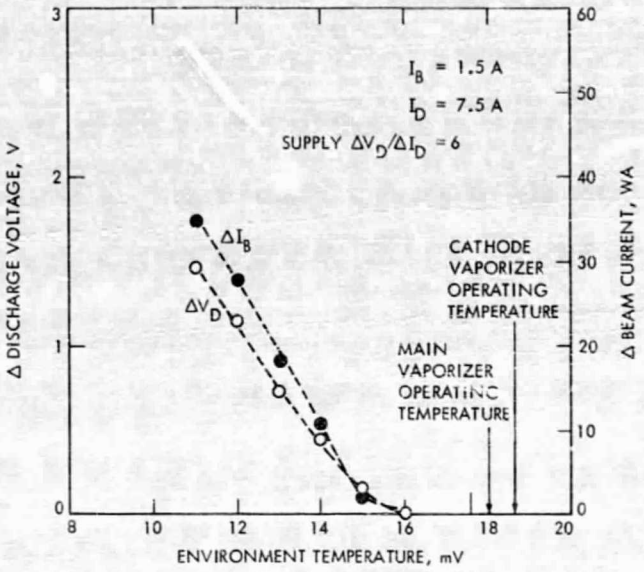

Fig. 18. Loop oscillations vs temperature at typical beam current (1.5 A)

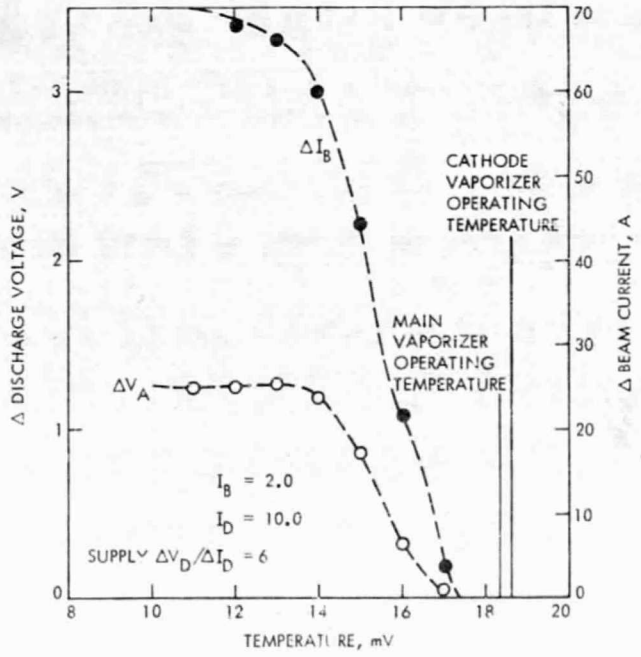

Fig. 19. Loop oscillations vs temperature at typical beam current (2.0 A)

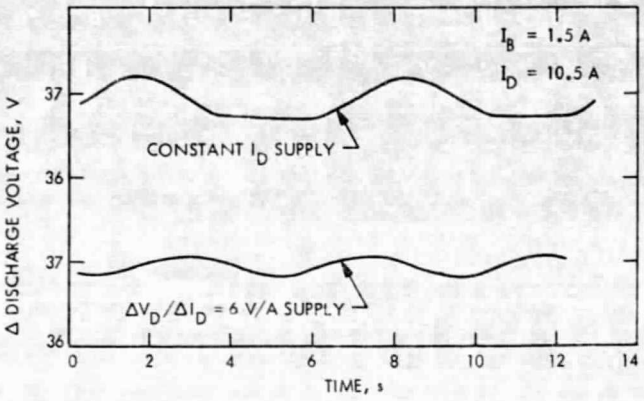

Fig. 20. Comparison of discharge voltage ripple

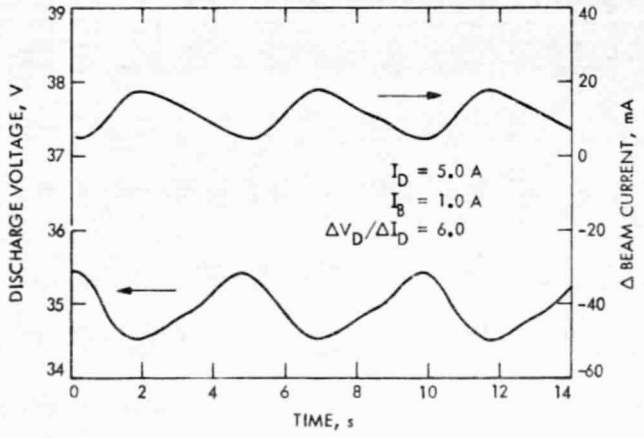

Fig. 21. Oscillations using a constant slope supply

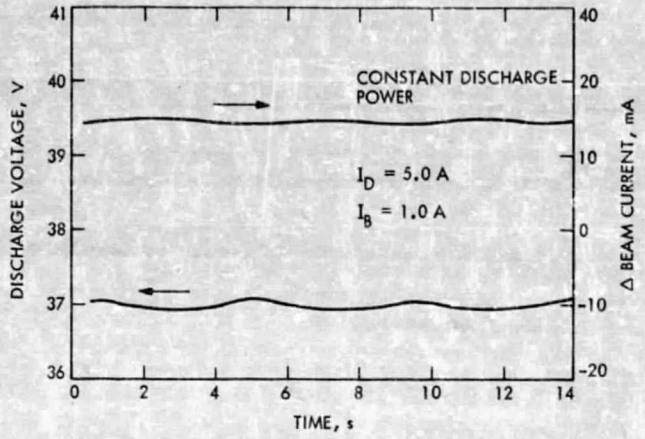

Fig. 22. Loop oscillations using a constant power supply

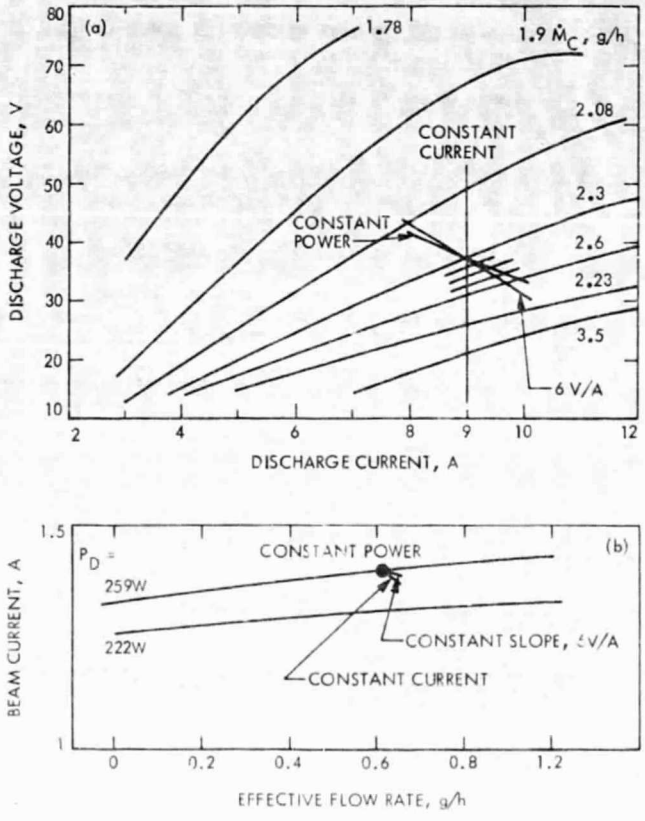

Fig. 23. Discharge supply characteristics plotted on thruster characteristics

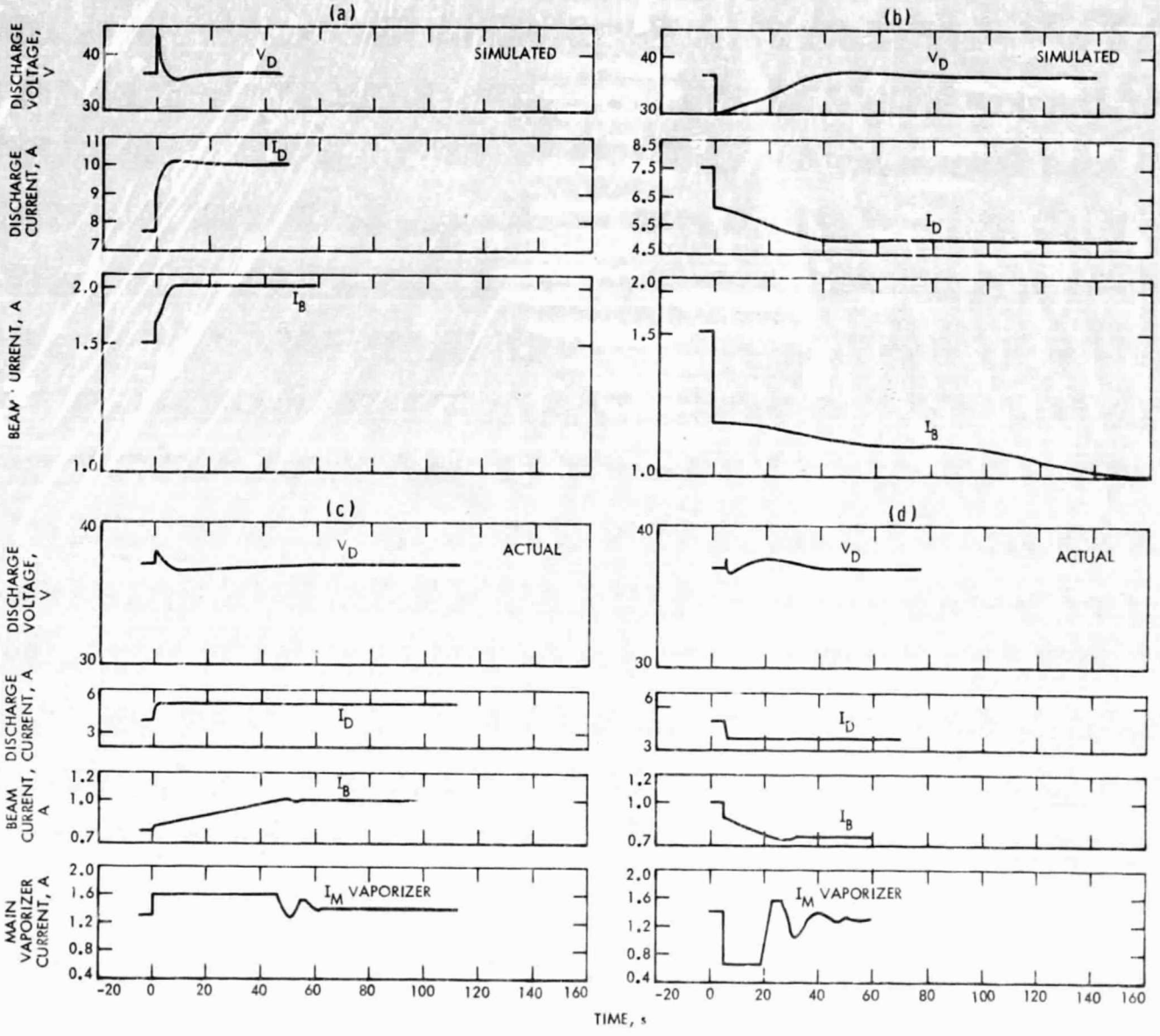

Fig. 24. Comparison of simulated and actual step responses

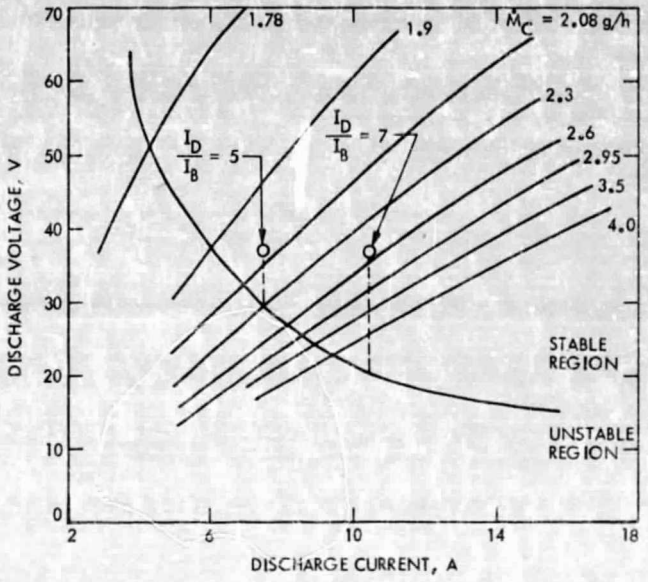

Fig. 25. Discharge characteristics showing the effect of I_D/I_B ratio

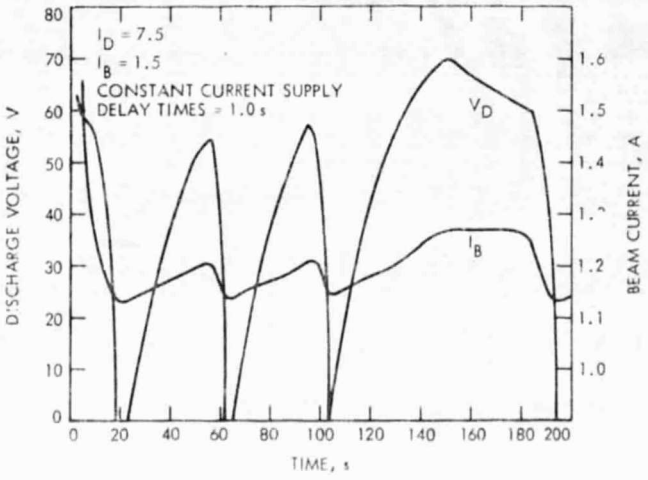

Fig. 26. Runaway recovery characteristics when using a constant current discharge supply

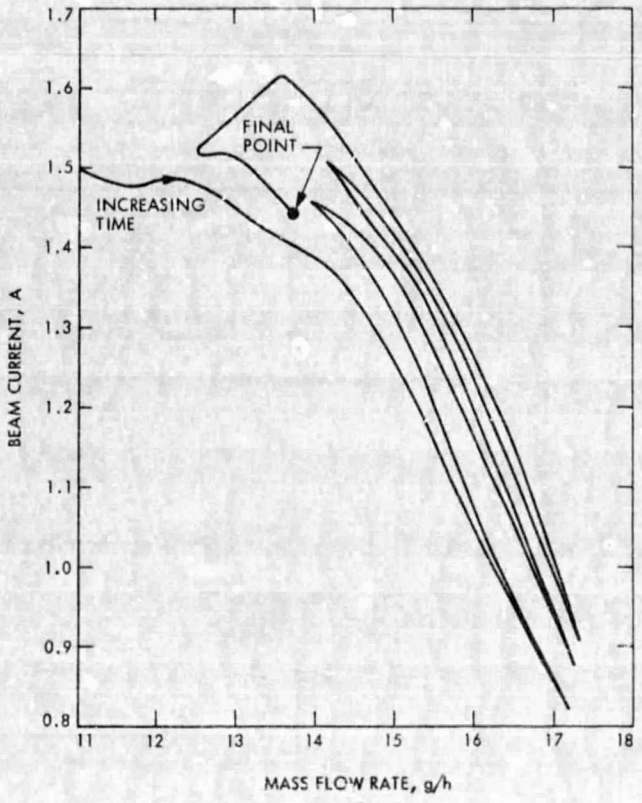

Fig. 27. Flow rate vs beam current for a constant discharge current supply

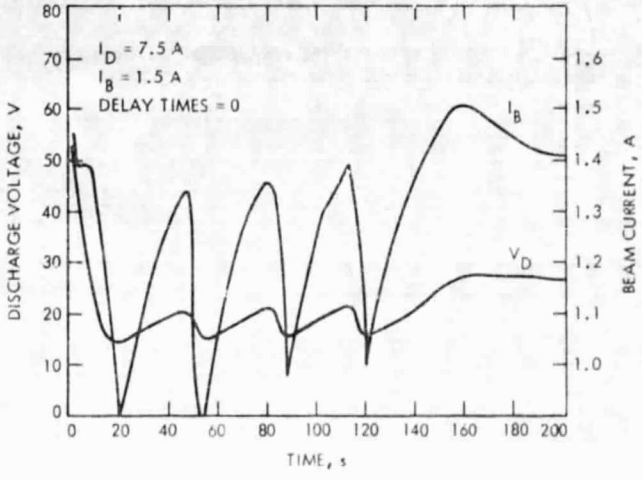

Fig. 28. Runaway recovery characteristics with zero delay times

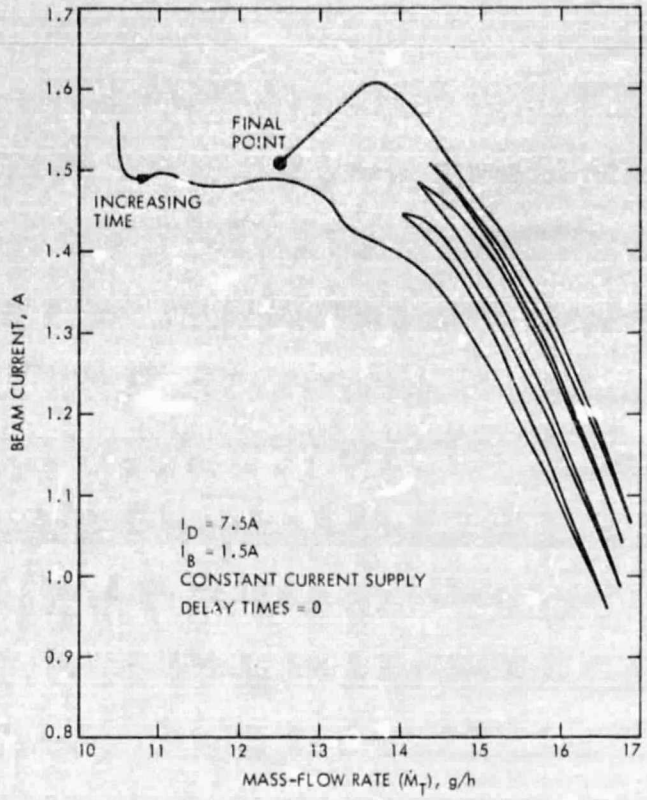

Fig. 29. Flow rate vs beam current

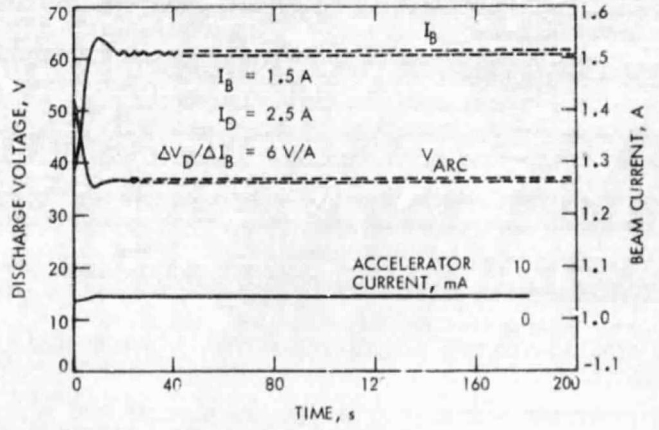

Fig. 30. Runaway recovery characteristics when using a 6 V/A discharge supply

APPENDIX A

COMPUTER-PROGRAM LISTING FOR THE ION THRUSTER MODEL

```
-ASG,A CSSL*TRAN
-XQT,G CSSL*TRAN.CSSL
      PROGRAM ION
      COMMENT  700 SERIES THRUSTER
      COMMENT THIS PROGRAM FORMS FINAL SHAPE
      COMMENT DEAD TIME  1SEC FOR MAIN LOOP
      COMMENT DEAD TIME 1 SEC FOR CATHODE LOOP
      COMMENT CONST SLOPE POWER SUPPLY
      COMMENT TIME CONST
      CONSTANT TAU1=210.0,TAU2=210.0, TAU3=210.0
      COMMENT TEMPERATURE-MOOT
      CONSTANT ALPHA1=0.35,B1=-7.0895
      CONSTANT ALPHA2=0.35,B2=-3.7625
      CONSTANT ALPHA3=0.35, B3=-7.0895
      COMMENT HEATER RESISTANCE=CONST OHM
      CONSTANT R=2.65
      COMMENT DISCHARGE CHAMBER CHARACTERISTICS
      CONSTANT VARCR=37.0
      COMMENT MASS OF MERCURY
      CONSTANT MHG=3.3E-25
      COMMENT BEAM CURRENT
      CONSTANT IBREF0=1.5
      COMMENT GAIN
      CONSTANT GAIN1R=1.0,GAIN2=-110.0,GAIN3R=1.0
      COMMENT CONTROL POINT
      CONSTANT C11=0.5, C12=0.5, C13=0.5, C21=2.0, C22=2.0, C23=2.0
      COMMENT NEUTRALIZER KEEPER CURRENT
      CONSTANT INKR=0.6
      COMMENT NEUTRALIZER KEEPER VOLTAGE
      CONSTANT VNKR=12.5
      COMMENT ENVIRONMENT TEMPERATURE
      CONSTANT TE1=15.0
      CONSTANT TE2=15.0
      CONSTANT TE3=13.0
      COMMENT MAIN FLOW ATTENUATION
      CONSTANT K=0.133
      CONSTANT Q1=1.6E-19
      CONSTANT Y00=2.5
      CONSTANT Y01=5.5
      CALL MAIN
      SEGMENT MAIN
      INITIAL
      PAGE EJECT
      TITLE T,VARC,IB,IACCEL,VNK,YETAU
      TITLE SMC,SMM,SMN,I1,I2,I3
      TITLE TC11,TC21,FLARC,MT,MC,IARC
      N1=1.0
      COMMENT ASSIGN CATH VAP HEATER INITIAL CURRENT
      I1IC=1.2 $ I11=1.2
      COMMENT ASSIGN MAIN VAP HEATER INITIAL CURRENT
      I2IC=0.8 $ I21=0.8
      COMMENT ASSIGN NEUT VAP HEATER INITIAL CURRENT
      I3IC=0.8 $ I31=0.8
      IARCRO=7.5
```

```
GAIN3=GAIN3R
ACCN=0.0
END
DYNAMIC
VARIABLE T=0.0
COMMENT NO CHANGE IN ARC CURRENT IN THIS CASE
ABRARC=0.0
IARCR=IARCRO-ABRARC
IBREF=IBREFO
COMMENT CATHODE VAP GAIN CHANGE
ABRG1=STEP(200.0,T)
ABRG2=STEP(400.0,T)
ABRG3=STEP(600.0,T)
ABRG4=STEP(800.0,T)
ABRG5=STEP(1000.0,T)
GAIN1=GAIN1R+ABRG1+ABRG2+ABRG3 ...
 ABRG4+ABRG5
COMMENT CALCULATE EACH VAP HEATER CURRENT
MACRO  MACRO HEATER Q
MACRO RELABEL L1,L2
IF(Q(4).GE.2.0) GO TO L1
Q(1)=Q(5) $ Q(2)=Q(6) $ Q(3)=Q(7)
GO TO L2
L1..Q(1)=Q(8) $ Q(2)=Q(9) $ Q(3)=Q(10)
L2..CONTINUE
MACRO END
HEATER I1,I2,I3,N1,I1IC,I2IC,I3IC,...
I11,I21,I31
W1=R*I1**2 $ W2=R*I2**2 $ W3=R*I3**2
STD1=TDW(W1) $ STD2=TDW(W2) $ STD3=TDW(W3)
IF(N1.GE.2.0) GO TO L3
TDX1=STD1 $ TDX2=STD2 $ TDX3=STD3
GO TO L4
L3..TDX10=TDX1 $ TDX20=TDX2 $ TDX30=TDX3
TD1=STD1 $ TD2=STD2 $ TD3=STD3
CALL INT(TDX10,TDX20,TDX30,TD1,TD2,TD3,TDX1,TDX2,TDX3)
L4..CONTINUE
COMMENT DUMMY INTEGRATION
DERIVATIVE DUM
SDUM=INTEG(0.0,0.0)
CINTERVAL CI=0.2
END
COMMENT VAPORIZER TEMPERATURE
TC11=TDX1+TE1
TC21=TDX2+TE2
TC31=TDX3+TE3
COMMENT MASS FLOW RATE
SMC=EXP(B1)*EXP(ALPHA1*TC11)
SMM=EXP(B2)*EXP(ALPHA2*TC21)
SMN=EXP(B3)*EXP(ALPHA3*TC31)
COMMENT DEAD TIME (TRANSPORTATION LAG)
IF(N1.GE.2.0) GO TO DD1
Y11=SMC $ Y21=SMC $ Y31=SMC
Y41=SMC $ Y51=SMC
```

```
Y61=SMC $ Y71=SMC $ Y81=SMC
Y91=SMC $ Y101=SMC
Y12=SMM $ Y22=SMM $ Y32=SMM
Y42=SMM $ Y52=SMM
Y13=SMN $ Y23=SMN $ Y33=SMN
Y43=SMN $ Y53=SMN
YE1=SMC $ YE2=SMM $ YE3=SMN
SSMC=YE1 $ SSMM=YE2 $ SSMN=YE3
GO TO DD2
DD1..CONTINUE
MACRO MACRO DEL1 U
MACRO REDEFINE YA1,YB1,YC1,YD1,YE1
MACRO REDEFINE YF1,YG1,YH1,YI1,YJ1
YA1=U(1) $ YB1=U(2) $ YC1=U(3)
YD1=U(4) $ YE1=U(5)
YF1=U(6) $ YG1=U(7) $ YH1=U(8)
YI1=U(9) $ YJ1=U(10)
U(11)=YE1
U(1)=U(12) $ U(2)=YA1 $ U(3)=YB1
U(4)=YC1 $ U(5)=YD1
U(6)=YE1 $ U(7)=YF1 $ U(8)=YG1
U(9)=YH1 $ U(10)=YI1
MACRO END
MACRO MACRO DEL2 UU
MACRO REDEFINE YA2 ,YB2,YC2,YD2,YE2
YA2=UU(1) $ YB2=UU(2) $ YC2=UU(3)
YD2=UU(4) $ YE2=UU(5)
UU(6)=YE2
UU(1)=UU(7) $ UU(2)=YA2 $ UU(3)=YB2
UU(4)=YC2 $ UU(5)=YD2
MACRO END
MACRO MACRO DEL3 UUU
MACRO REDEFINE YA3,YB3,YC3,YD3,YE3
YA3=UUU(1) $ YB3=UUU(2) $ YC3=UUU(3)
YD3=UUU(4) $ YE3=UUU(5)
UUU(6)=YE3
UUU(1)=UUU(7) $ UUU(2)=YA3 $ UUU(3)=YB3
UUU(4)=YC3 $ UUU(5)=YD3
MACRO END
DEL1 Y11,Y21,Y31,Y41,Y51,Y61,Y71,Y81,Y91,Y101,SSMC,SMC
DEL2 Y12,Y22,Y32,Y42,Y52,SSMM,SMM
DEL3 Y13,Y23,Y33,Y43,Y53,SSMN,SMN
DD2..CONTINUE
MC=SSMC+K*SSMM
MT=SSMC+SSMM
MN=SSMN
COMMENT TABLE OF VAPORIZER TEMPERATURE CHANGE CORRESPONDING TO
TABLE TDW,1,6, ...
0.0,1.5, 3.5, 6.0, 9.0, 10.6, ...
0.0,2.0, 5.5, 10.5,17.5,23.0
COMMENT ARC CHAMBER CHARACTERISTICS
TABLE ARCMC,2,7,7, ...
1.78,1.9,2.08,2.3,2.6,2.95,3.5,...
3.0,5.0, 7.0, 9.0, 11.0,13.0,15.0,...
```

```
37.0,13.5,3.0,0.0,0.0,0.0,0.0,...
61.5,37.0,26.5,20.0,15.0,10.5,6.5,...
76.0,52.0,37.0,26.7,23.5,18.8,14.5,...
90.0,67.0,48.0,37.0,30.3,25.5,21.0,...
102.0,77.0,58.5,45.0,37.0,30.7 27.0,...
111.0,86.0,67.0,53.7,43.5,37.0,32.0,...
118.0,93.0,72.0,60.0,50.5,42.5,37.0
COMMENT BEAM CHARACTERISTICS
TABLE IBMT,2,22,7,...
0.0,4.0,5.0,6.0,7.0,8.0,9.0,10.0,11.0,12.0,...
13.0,14.0,15.0,16.0,17.0,18.0,19.0,20.0,21.0,22.0,...
23.0,24.0,...
111.0,148.0,185.0,222.0,259.0,296.0,333.0,...
0.0,0.37,0.49,0.60,0.66,0.71,0.74,0.75,0.74,0.71,...
0.66,0.60,0.52,0.39,0.25,0.08,-0.15,-0.47,-0.67,-0.95,...
 1.23,-1.50,...
0.0,0.42,0.54,0.63,0.74,0.82,0.86,0.92,0.97,1.00,...
0.99,0.96,0.91,0.84,0.66,0.71,0.35,0.15,-0.14,-0.36,...
 0.60,-0.85,...
0.0,0.42,0.55,0.67,0.80,0.91,1.00,1.09,1.13,1.18,...
1.20,1.16,1.13,1.04,0.96,0.84,0.73,0.64,0.50,0.35,...
0.23,0.16,...
0.0,0.45,0.57,0.70,0.83,0.97,1.08,1.16,1.26,1.33,...
1.37,1.41,1.42,1.41,1.39,1.33,1.26,1.16,1.05,0.95,...
0.85,0.74,...
0.0,0.47,0.61,0.74,0.85,0.97,1.12,1.24,1.34,1.43,...
1.51,1.55,1.60,1.61,1.63,1.61,1.56,1.55,1.50,1.43,...
1.35,1.26,...
0.0,0.47,0.61,0.74,0.85,0.97,1.12,1.25,1.36,1.49,...
1.60,1.69,1.76,1.83,1.90,1.96,2.00,2.04,2.06,2.09,...
2.10,2.09,...
0.0,0.47,0.61,0.74,0.85,0.97,1.13,1.27,1.41,1.54,...
      1.66,1.77,1.90,1.99,2.10,2.20,2.30,2.40,2.51,2.61,...
2.71,2.74
COMMENT NEUT KEEPER CHARACTERISTICS
TABLE NKMN,2,6,4, ...
0.6,0.7,0.8, 0.9, 1.0, 1.1, ...
0.31,0.36,0.41,0.46, ...
13.5,13.5,13.5,13.5,13.5,13.5, ...
13.0,13.0,13.0,13.0,13.0,13.0, ...
12.5,12.5,12.5,12.5,12.5,12.5, ...
12.0,12.0,12.0,12.0,12.0,12.0
NEG=1.0
IF(NEG.LT.0.0) GO TO LNEG
COMMENT NEUT POWER SUPPLY CHARCTERISTICS
YOIARC=7.0
SLOPMC=6.0
IARC=IMPL(YOIARC,0.001,20,FLARC,IARCR+...
(VARCR-ARCMC(MC,IARC))/SLOPMC,0.01)
LNEG..CONTINUE
VARC=ARCMC(MC,IARC) $ PARC=VARC*IARC
IB=IBMT(MT,PARC)
YOINK=0.5
SLOPNK=30.0
```

```
INK=IMPL(YOINK,0.001,20,FLNK,INKR+...
(VNKR-NKMN(INK,MN))/SLOPNK,0.01)
VNK=NKMN(INK,MN)
COMMENT CATHODE VAPORIZER CONTROLLER
V1=(C11-C21)/(2.0*GAIN1)+VARCR
V2=(C21-C11)/(2.0*GAIN1)+VARCR
                PROCEDURAL(I11=V1,V2,VARC,VARCR,C11,C21,GAIN1)
                IF(VARC.LT.V1) I11=C11
IF((VARC.GE.V1).AND.(VARC.LE.V2)) I11=...
GAIN1*VARC-GAIN1*VARCR+(C11+C21)/2.0
IF(VARC.GT.V2) I11=C21
                END
COMMENT MAIN VAPORIZER CONTROLLER
DIB=IB-IBREF
DIB2=(C12-C22)/GAIN2
                PROCEDURAL(I21=DIB2,DIB,C12,C22,GAIN2)
IF((DIB.GE.0.0).AND.(DIB.LT.DIB2)) I21=...
                GAIN2*DIB+C22
IF(DIB.LT.0.0) I21=C22
IF(DIB.GE.DIB2) I21=C12
                END
    COMMENT NEUTRALIZER VAPORIZER CONTROLLER
VNK1=(C13-C23)/(2.0*GAIN3)+VNKR
VNK2=(C23-C13)/(2.0*GAIN3)+VNKR
                PROCEDURAL(I31=VNK,VNK1,VNK2,C13,C23,GAIN3,VNKR)
                IF(VNK.LT.VNK1) I31=C13
IF((VNK.GE.VNK1).AND.(VNK.LT.VNK2)) I31=...
GAIN3*VNK-GAIN3*VNKR+(C13+C23)/2.0
                IF(VNK.GE.VNK2) I31=C23
                END
COMMENT ACCEL CURRENT INTERRUPTION
IO=Q1*MT/MHG*1.0E-3/3600.0 $ YETAU=IB/IO
TABLE ACYETA,1,10,...
0.1,0.2,0.3,0.4,0.5,0.6,0.7,0.8,0.9,1.0,...
0.025,0.0199,0.015,0.0112,0.0086,...
0.0066,0.005,0.0037,0.0029,0.0022
IACCEL=ACYETA(YETAU)*IB
IF(IACCEL.GE.0.010) GO TO ACI1
IF(IACCEL.GE.0.006.AND.IACCEL.LT.0.010.AND.ACCN.EQ.1.0) GO TO ...
ACI1
IF(IACCEL.GE.0.006.AND.IACCEL.LT.0.010.AND.ACCN.EQ.0.0) GO TO  ...
ACI3
 IF(IACCEL.LT.0.006) GO TO ACI2
ACI1..I21=0.0 $ ACCN=1.0
 GO TO ACI3
ACI2..ACCN=0.0
ACI3..CONTINUE
IF(T.LT.20.0) GO TO LW2
IF(T.GE.180.0.AND.T.LT.200.0) GO TO LW2
IF(T.GE.360.0.AND.T.LT.400.0) GO TO LW2
IF(T.GE.580.0.AND.T.LT.600.0) GO TO LW2
IF(T.GE.780.0.AND.T.LT.800.0) GO TO LW2
IF(T.GE.980.0.AND.T.LT.1000.0) GO TO LW2
IF(T.GE.1180.0.AND.T.LT.1200.0) GO TO LW2
```

```
      WDUM=1.0 $ GO TO LW1
      LW2..CONTINUE
      OUT T,VARC,IB,IACCEL,VNK,YETAU,C1
      OUT SMC,SMM,SMN,I11,I21,I31,C1
      OUT TC11,TC21,FLARC,MI,MC,IARC,C1
      PAGE SKIP,1,C1
      LW1..CONTINUE
      IF(IB.LE.0.0) GO TO L5
      IF(T.GE.400.0) GO TO L5
      N1=2.0
      END
      TERMINAL
      L5.. CONTINUE
      END
      END
      COMMENT FIRST ORDER LAG TRANSFER FUNCTION
      SEGMENT INT(TDX10P,TDX20P,TDX30P,TD1P,TD2P,TD3P,...
      TDX1P,TDX2P,TDX3P)
      INITIAL
      NN=0.0
      V=0.0
      TDX1Q=TDX1P $ TDX2Q=TDX2P $ TDX3Q=TDX3P
      TD1Q=TD1P $ TD2Q=TD2P  $ TD3Q=TD3P
      TDX10Q=TDX10P $ TDX20Q=TDX20P $ TDX30Q=TDX30P
      END
      DYNAMIC
      VARIABLE V=0.0
      IF(V.GE.0.2) GO TO L6
      DERIVATIVE SINT
      TDX1Q=REALPL(TAU1,TD1Q,TDX10Q)
      TDX2Q=REALPL(TAU2,TD2Q,TDX20Q)
      TDX3Q=REALPL(TAU3,TD3Q,TDX30Q)
      CINTERVAL CIP=0.2
      NN=1.0
      END
      END
      TERMINAL
      L6..CONTINUE
      TDX1P=TDX1Q $ TDX2P=TDX2Q $ TDX3P=TDX3Q
      TD1P=TD1Q $ TD2P=TD2Q $ TD3P=TD3Q
      TDX10P=TDX10Q $ TDX20P=TDX20Q $ TDX30P=TDX30Q
      END
      END
      END
-FIN                                                          NIF-
```